ELSEVIER

Synthesis and processing of SOFC components for the fabrication and characterization of anode supported cells

Aritza Wain-Martin [a], Roberto Campana [b,*], Aroa Morán-Ruiz [a], Aitor Larrañaga [a], María Isabel Arriortua [a,c]

[a] *Universidad del País Vasco (UPV/EHU), Facultad de Ciencia y Tecnología, Barrio Sarriena S/N, 48940 Leioa, Spain*
[b] *Centro Nacional del Hidrógeno, Prolongación Fernando el Santo s/n, 13500 Puertollano, Ciudad Real, Spain*
[c] *BCMaterials, Basque Center for Materials, Applications and Nanostructures, Bld. Martina Casiano, 3rd. Floor UPV/EHU Science Park, Barrio Sarriena s/n, 48940 Leioa, Spain*

ARTICLE INFO

ABSTRACT

In this article, it is intended to evaluate the performances of previously synthesized different nanometric compounds as SOFC components under real conditions. For this purpose, anodic supports SOFCs have been manufactured in different configurations.

The compounds NiO-$(Y_2O_3)_{0.08}(ZrO_2)_{0.92}$ (NiO–YSZ), $(Y_2O_3)_{0.08}(ZrO_2)_{0.92}$ (YSZ), $Sm_{0.2}Ce_{0.8}O_{1.9}$ (SDC), $La_{0.6}Sr_{0.4}FeO_3$ (LSF) and $LaNi_{0.6}Fe_{0.4}O_3$ (LNF) were used as anode support, electrolyte, barrier, cathode and contact layer, respectively. To obtain the cells, the anode supports were produced by uniaxial pressing and the remaining layers were added using the airbrush technique, assembling them by different sintering processes. The cells developed have been electrochemically tested in a temperature range between 750 and 865 °C. Additionally, degradation tests have been carried out under constant current. Moreover, to characterize the microstructure of the cells, a scanning electron microscope (SEM) equipped with an energy dispersive X-ray spectroscopy (EDX) analyzer has been used.

The results obtained show that the incorporation of cathode and contact layers increases the power densities and decreases the total resistances of the cells with respect to the cell without cathode, especially with the addition of the LNF contact layer. Despite the improvement obtained, more tests have to be carried out in order to optimize the performance of SOFC devices in degradation tests.

* Corresponding author.
E-mail address: roberto.campana@cnh2.es (R. Campana).

Síntesis y procesado de componentes SOFC para la fabricación y caracterización de celdas de soporte anódico

R E S U M E N

Palabras clave:
Celdas de combustible de óxido sólido
Procesado
Composite
Degradación
Espectroscopía de impedancia electroquímica

En el presente artículo se pretende evaluar el rendimiento de diferentes compuestos nanométricos previamente sintetizados como componentes pila de combustible de óxido sólido (SOFC) en condiciones reales. Para ello se han fabricado pilas SOFC de soporte anódico con distintas configuraciones.

Los compuestos NiO-$(Y_2O_3)_{0.08}(ZrO_2)_{0.92}$ (NiO–YSZ), $(Y_2O_3)_{0.08}(ZrO_2)_{0.92}$ (YSZ), $Sm_{0.2}Ce_{0.8}O_{1.9}$ (SDC), $La_{0.6}Sr_{0.4}FeO_3$ (LSF) y $LaNi_{0.6}Fe_{0.4}O_3$ (LNF) se utilizaron como soporte anódico, electrolito, barrera, cátodo y capa de contacto, respectivamente. Para la obtención de las celdas, los soportes anódicos se fabricaron mediante prensado uniaxial y las capas restantes se añadieron utilizando la técnica de aerografía, ensamblándolas mediante diferentes procesos de sinterización. Las celdas desarrolladas se han testeado electroquímicamente en un rango de temperaturas entre 750 y 865 °C. Además, se han llevado a cabo ensayos de degradación bajo corriente constante. Asimismo, para caracterizar la microestructura de las celdas, se ha utilizado un microscopio electrónico de barrido (SEM) equipado con un espectrómetro de rayos X por energía dispersiva (EDX).

Los resultados obtenidos muestran que la incorporación de las capas catódicas y de contacto incrementan las densidades potencia y disminuyen las resistencias totales de las celdas respecto a la celda sin cátodo, especialmente al añadir la capa de contacto LNF. A pesar de la mejora obtenida, se han de realizar más ensayos a fin de optimizar el funcionamiento de los dispositivos SOFC en los ensayos de degradación.

Introduction

During the last decades, the global warming and the raise in energy demands have led to a growing interest in cleaner and more efficient power systems to face the shortage of fossil fuels [1]. Currently, solid oxide fuel cells (SOFCs) have become relevant as energy conversion devices since they are an efficient and ecofriendly technology, as well as they can use different types of fuel, transforming the chemical energy of hydrogen or other fuels, such as biogas, light hydrocarbons or even kerosene, into electrical power and heat, reducing the greenhouse gas emissions [2,3]. Among the different types of configurations for SOFCs systems, planar ones are promising, because their fabrication cost is cheaper and their manufacturing process is simpler comparing with tubular SOFCs [4,5]. On the other hand, the anode supported cells, allow lowering the electrolyte thickness, reducing the ohmic losses and thus, increasing the power density of the systems [6]. Among the main limitations for the commercialization of SOFC, are their high manufacturing costs and short operation life, which are an obstacle for their industrial implementation [7].

In order to face these problems, researchers have attempted to decrease the fabrication cost of SOFCs and increase the operation time by reducing the operation temperature, reducing the sintering temperature during the fabrication, reducing the number of thermal cycles or optimizing the microstructures [8–11]. In correlation with this, significant improvements in degradation can be achieved by controlling the grain size of the starting powders. The use of nanoparticles has demonstrated to enhance the catalytic activity of the components, giving the possibility to operate at lower temperatures, reducing the energy consumption in thermal cycles and controlling the microstructure of the components [12–14]. Wet chemical synthesis methods, such as hydrothermal synthesis [15] or oxalate co-precipitation [16], can produce oxide powders with homogeneous distribution of elements, large surface areas and well defined chemical compositions. The problem with these methods is that, despite the quality of the powders produced, the processes are complicated and take long periods of time, limiting their applicability. On the other hand, the synthesis by combustion method using metal nitrates and glycine, urea, citric acid, etc., as fuel, has proven to produce homogeneous, crystalline, very fine and nanometric grain size powders in a simple and economical way [17–19].

In addition, the complex and expensive different processing stages for anode-supported electrolyte tapes could be replaced by simpler, more economical and continuous techniques. Among the composite layers deposition methods, wet powder spraying is a mature technology and a reasonably cost-effective process. Although it was initially used to create porous ceramic layers, it is possible to produce dense thin films, being possible to control the quality and the thickness of cell layers. Additionally, this method is suitable for planar or tubular surfaces, as well as is easily automatable and industrially scalable, since presents a highly reproducible process [20–22].

In the development of SOFCs, the use of metal oxides is very common, specially perovskites, such as (La,Sr)MnO₃

(LSM) or (La,Sr)CoO$_3$ (LSC) cathodes [23,24]. The utilization of (La,Sr)FeO$_3$ (LSF) instead the most commonly used cathodes, is an attractive change, since these phases have good catalytic and conductive properties between 600 and 800 °C and shows proper thermal compatibility with YSZ electrolytes. The use of ceria based materials (as Ce$_{0.8}$Gd$_{0.2}$O$_{1.9}$ (GDC) or Ce$_{0.8}$Sm$_{0.2}$O$_{1.9}$ (SDC)) must also be taken into account to be used as a reaction barrier between the electrolyte and the cathode, avoiding the formation of secondary phases such as La$_2$Zr$_2$O$_7$ or SrZrO$_3$ which generate ohmic conductivity losses [25,26]. Is also interesting to add cathode contact layers such as LaNi$_{0.6}$Fe$_{0.4}$O$_3$ (LNF) or LaNi$_{0.6}$Co$_{0.4}$O$_3$ (LNC), which have demonstrated to improve the electrical contact between the interconnect and the cathode, reducing the stack power losses and ohmic interfacial resistances [27,28].

The current work describes the characterization of self-synthesized SOFC components [29] (Ni–YSZ, YSZ, SDC, LSF and LNF) processing them in different cell configurations and characterizing the contribution of each one. Composite layers (between the SDC and LSF; and LSF and LNF) have been added by mixing both components to overcome the mismatches of thermal expansion coefficients (TEC) between the layers. For the fabrication process, the anode support was carried out via uniaxial pressing, while the deposition of the remaining layers was made by manual spray coating. The microstructure was characterized by scanning electron microscopy (SEM) and energy dispersive X-ray spectroscopy (EDX). The electrochemical response of this assembly was studied using current–voltage (*I*–*V*) curves, current–power (*I*–*P*) curves and electrochemical impedance spectroscopy (EIS). To conclude this study, an investigation of a short-term degradation phenomenon has been done, performing constant current measurements. In this study, the feasibility of our self-synthesized compounds as SOFCs components after their manufacture has been demonstrated and the use of different cell components is discussed.

Experimental

Synthesis and cell fabrication

The NiO–YSZ, YSZ, SDC, LSF and LNF components were prepared by glycine nitrate combustion method. In all the cases, glycine was added to the aqueous nitrate solution while stirring, being the nitrate glycine molar ratio 1. The resulting viscous liquid was auto-ignited and heated up to 455 °C. The carbon residues were removed by calcining the obtained powders between 600 and 800 °C for 5 h, obtaining pure samples. The characteristics (crystal structure, particle size or TEC) and synthesis process of the powders are detailed elsewhere [29].

The anode supports were manufactured by uniaxial pressing and the deposition of all the films was carried out using manual spray coating. The anode was made with a NiO/YSZ ratio of 63 wt%/37 wt%, a 18 mm diameter, a thickness of 800 μm and a final porosity of 40% using starch as pore former, before NiO reduction. The anode pellets were presintered in air at 600 °C for 2 h, before being used as supports for YSZ spraying. This thermal treatment was adequate to provide a mechanical resistance without causing a significant

Table 1 – Details of the created cells.

Sample name	Layer	Thickness
Cell 1	Ni–YSZ	800 μm
	YSZ	20 μm
Cell 2	Ni–YSZ	800 μm
	YSZ	20 μm
	SDC	5 μm
	SDC–LSF	20 μm
	LSF	75 μm
Cell 3	Ni–YSZ	800 μm
	YSZ	20 μm
	SDC	5 μm
	SDC–LSF	20 μm
	LSF	20 μm
	LSF/LNF	15 μm
	LNF	20 μm

shrinkage. Before deposition, the powders of each component were ball milled at 270 rpm for 24 h using 2-propanol as solvent and adding a 4% of surfactant (PVP K15, Sigma Aldrich) versus total powder. The thickness was controlled by checking the added weight and considering the density of the deposited compounds. When the electrodes were sprayed, they were shaped to have a diameter of 12 mm. The sintering of the thin and fully dense YSZ electrolyte layer (20 μm) was carried out at 1400 °C for 2 h, while the remaining layers were sintered separately at 1150 °C for 2 h.

In this work, three types of cells were fabricated and characterized, which are described in Table 1. The cell 1 was made out with an anode support and an YSZ layer. In the cell 2, SDC, SDC–LSF composite, and LSF cathode layers were added. Finally, considering the previous results, in the cell 3, LSF–LNF composite and LNF contact layers were added to the previous multilayer cell sequence. The schematic structure of the manufactured cells is shown in Fig. 1.

The complexity of the cells was increased in order to study the effect of the new layers on the system. The difference between cell 2 and cell 3 is that the total thickness of the cathode side was slightly decreased replacing 75 μm of LSF (cell 2) by 20 μm, 15 μm and 20 μm of LSF, LSF/LNF and LNF, respectively (cell 3). In each configuration, the aim is to evaluate the performance of the synthesized oxides in real operation.

To study the microstructure, the cross sections of the cells were examined using scanning electron microscopy (SEM). The compositional analysis was made using back-scattered electrons (BSE) at an accelerating voltage 20 kV and a current of 5 × 10−9 A.

Electrochemical characterization

In order to perform the electrochemical tests, Pt paste was added into the cathode and anode of each sample to improve the contact between the cells and Pt wires and the cells were mounted on a button-cell test rig (NorECs Probostat, Norway) attached by a spring-loaded mechanism. Then, in order to separate the anode and cathode chambers, Omegabond 700 high temperature cement was used. Electrochemical measurements were collected employing a multichannel Potentiostat/Galvanostat VMP3 (Biologic), using humidified H$_2$

Fig. 1 – Scheme of the used layers in each cell.

(~3 vol% H_2O) as fuel gas on the anodic side and air on the cathodic one at temperatures of 750, 800 and 865 °C. The flow rates were set at 15 ml/min for H_2 and Q < 200 ml/min for air.

To distinguish between different contributions to the total resistance, the collected data were treated with the ZPlot 3.5b software using the equivalent electrical diagram presented in Fig. 2. R_s represents the pure ohmic resistance. Each of the parallel resistance circuits and constant phase elements gives account for its respective high to low frequency depressed semicircle. The elements contribute to the impedance from left to right in the Nyquist diagrams in decreasing frequency. L inductance has been added to take into consideration the equipment contribution in the measurements. R_{Total} is calculated from $R_{Total} = R_p + R_s$ formula, where R_p is the polarization resistance, the resistance given by the sum of the high and low frequency Nyquist plot semicircles ($R_{HF} + R_{LF}$).

To calculate the relaxation frequency for each contribution, the following equation has been applied [30]:

$$C = \left(R^{1-n}Q\right)^{1/n} \tag{1}$$

$$f_0 = \frac{(RQ)^{-1/n}}{2\pi} \tag{2}$$

where R, Q and n values are obtained from the impedance data fitting according to the equivalent circuit shown in Fig. 2.

Stability study

The integrity of the cells was analyzed by performing operation test under constant current for at least 40 h at 100 mA/cm². Subsequently, post mortem analyses of the cells after the degradation test were evaluated by SEM and EDX mapping. The EDX live time was set to 100 s and the calibration

system was carried out by measuring the beam current in pure element standards, allowing the quantitative elemental analysis. Moreover, the EDX mapping was done using 13,762.56 s (70 ms/pixel) as live time. The data obtained were treated using Oxford INCA nanoanalysis software and the used specific emission lines for EDX analysis were K_α for Ni and Fe and L_α for La, Fe, Zr, Sm and Ce.

Results and discussion

Cell fabrication

In Fig. 3 are shown the surface and cross section micrographs for a sample identical to the cell 1 before electrochemical testing. In anode supported cells, obtaining the desired cell flatness is more difficult than in the case of electrolyte supported cells, due to the different shrinkages between the anode and electrolyte at high sintering temperatures [31]. Moreover, another added challenge is to create a dense layer on top of a porous support without losing adhesion between them. These challenges have been overcome and from the micrographs it could be concluded that the YSZ electrolyte layer presented the desired microstructure, with smaller than one micron closed pores and enough density to avoid the passage of gases through it. As can be seen in Fig. 3b, the contact between both layers proved to be adequate and the flatness of the cell was also correct. In this way, spray coating has proven to be an effective method to create thin and dense electrolyte layers.

Once the density of the electrolyte was tested, the function of the self-synthesized cathode powders in the cell arrangement was analyzed. In order to improve the thermal compatibility between different layers, a LSF/SDC composite film has been added between SDC barrier and LSF cathode layers, decreasing thermal mismatches. In Fig. 4, a SEM micrograph of the cathode side is shown, using a 15 μm
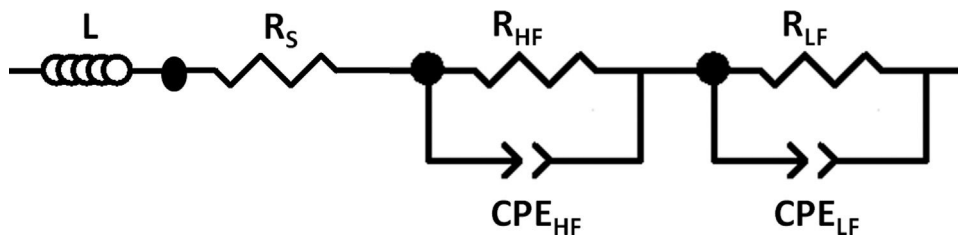
Fig. 2 – Equivalent circuit employed to fit impedance data.
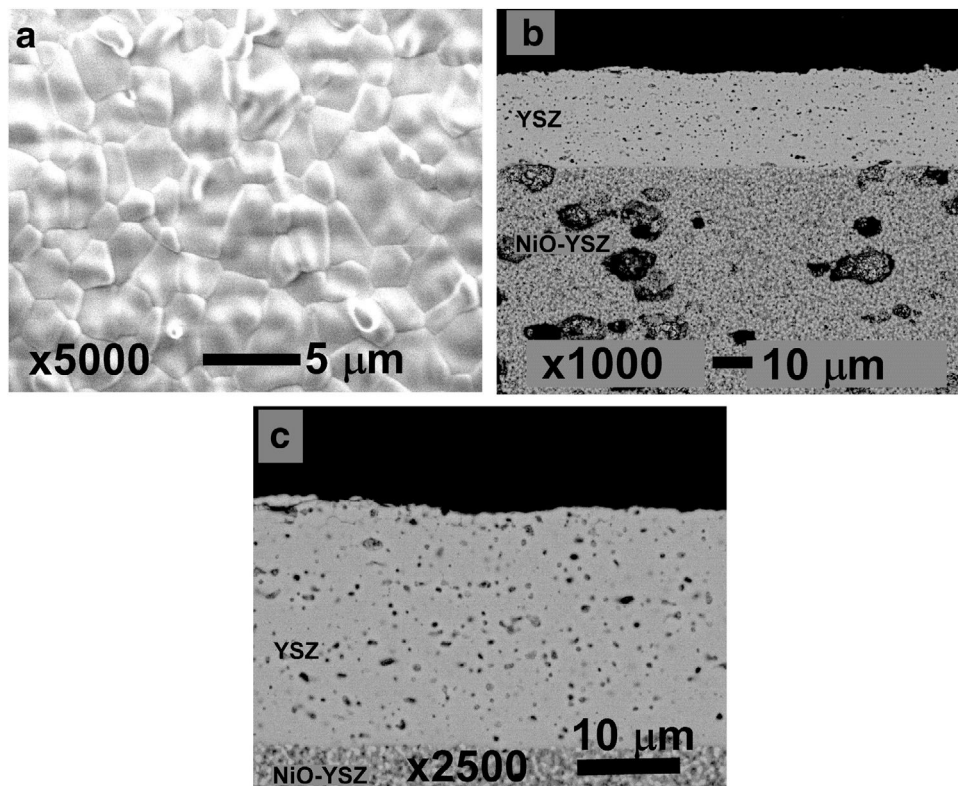
Fig. 3 – Micrographs of (a) the surface and (b and c) cross section morphology of the electrolyte layer.
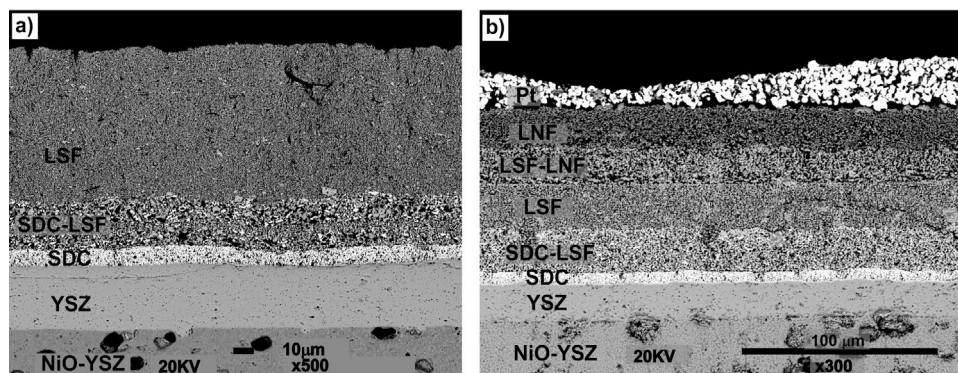
Fig. 4 – Micrograph of the cross section morphology of the cathode side in cell 2 (a) and cell 3 (b).

thickness SDC/LSF composite layer. As can be seen, no cracks or delaminations have been detected in the LSF layer and good adhesion between LSF and SDC layers is observed. Regarding the electrodes, they presented good thickness homogeneity and the expected porous microstructure.

Finally, LSF/LNF composite and LNF layers have been deposited onto the cathode in order to determine the effect of the contact layer on the cell. As in the previous cell, the layers have remained continuous, retaining their adhesion despite having increased their thickness. In addition, the added
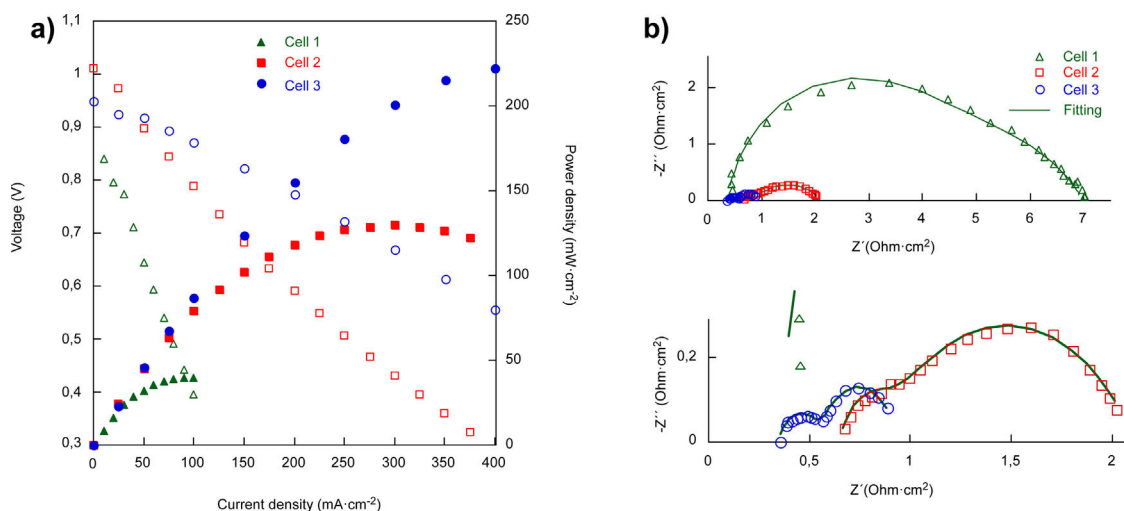
Fig. 5 – (a) (I–V–P) curves and (b) EIS of the cells 800 °C.

Table 2 – Maximum power densities for the cells at different temperatures.

Cell	Temperature (°C)	Maximum power (mW cm^{-2})
1	750	17
	800	40
	865	123
2	750	90
	800	130
	865	191
3	750	175
	800	222
	865	272

layers presented a microstructure suitable for their use as contact layer.

Electrochemical characterization

For the electrochemical characterization, platinum paste was used to improve the current collection, in addition to being used as cathode in the case of the cell 1. The current–voltage and current–power characteristics of the cells (1 cm^2 effective area) at 800 °C are given in Fig. 5a. The obtained open circuit voltage (OCV) are slightly lower than the predicted by the Nernst equation. Probably due to small leakages in the ceramic paste used as sealant. As Fig. 3 shown the YSZ electrolyte layer was dense enough in all the cases, without gas cross over and cracks [32]. The power densities of the cells at 800 °C increased

with the addition of layers, reaching 40, 130 and 222 mW cm^{-2}, for cell 1, cell 2 and cell 3, respectively.

Table 2 shows the maximum power densities obtained for cells 1, 2 and 3 at 750, 800 and 865 °C. As it can be seen, the maximum power density increases as the temperature increases, as well as when the cell complexity increases.

Fig. 5b shows the electrochemical impedance spectra (EIS) at 800 °C for the three cells and the results obtained for the fitting using the Zview software, which are collected in Table 3. From the EIS spectra, is possible to obtain the ohmic resistance (R_s) and the total resistance (R_{Total}), using the intersection values with the Z_{re} axis at high and low frequencies, respectively. This includes the ohmic resistance related to the electrodes, the electrolyte and the interfaces.

As expected, the ohmic resistance, mainly associated with the YSZ electrolyte, remained almost constant for the three cells while the total resistance of the cells decreased when increasing the complexity of the fabricated cell, from 6.99 to 0.941 Ω cm^2 in cell 1 and cell 3, respectively, at 800 °C. In order to separate the different contributions to the total resistance, the equivalent electrical diagram showed in Fig. 2 was used. The obtained values for the fitting in the cell 1, showed that the polarization resistance, calculated as ($R_{Total} - R_s$), was composed of two contributions of similar magnitude, 3.54 and 3.12 Ω cm^2, with an inverse relaxation time of 3800 and 480 Hz, respectively. From these results, it has not been possible to separate the processes associated with the low frequencies using the purposed equivalent circuit. In this way, it has been concluded that the low frequency contribution ($\leq$10 Hz),

Table 3 – Polarization resistances, frequencies and capacitances derived from the EIS fits at 800 °C.

Cell	R_s (Ω cm^2)	R_{HF} (Ω cm^2)	C_{HF} (F cm^{-2})	f_{HF} (Hz)	R_{LF} (Ω cm^2)	C_{LF} (F cm^{-2})	f_{LF} (Hz)	R_p (Ω cm^2)	R_{Total} (Ω cm^2)
1	0.330	3.542	1.2×10^{-5}	3800	3.12	1.1×10^{-4}	480	6.66	6.99
2	0.550	0.458	5.1×10^{-4}	683	1.10	6.2×10^{-2}	2.34	1.56	2.10
3	0.348	0.225	3.1×10^{-3}	231	0.368	0.838	0.516	0.593	0.941
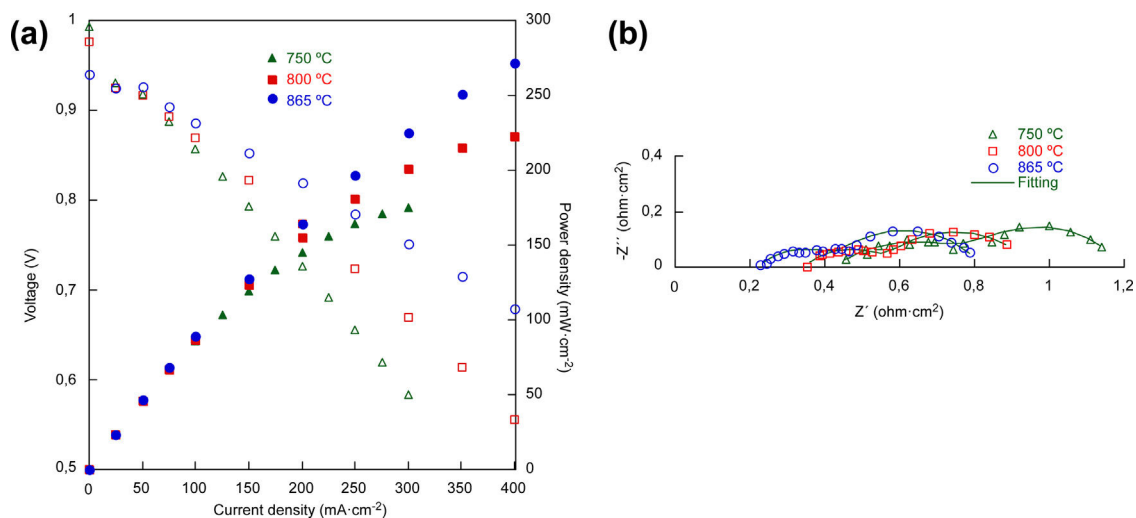
Fig. 6 – (a) (*I–V–P*) curves and (b) electrochemical impedance spectra of the sample cell 3 at 750, 800 and 865 °C, using Pt paste as electrode.

Table 4 – Polarization resistances, frequencies and capacitances obtained from the EIS of the cell 3 at 750, 800 and 865 °C.

T (°C)	R_s ($\Omega\,cm^2$)	R_{HF} ($\Omega\,cm^2$)	C_{HF} ($F\,cm^{-2}$)	f_{HF} (Hz)	R_{LF} ($\Omega\,cm^2$)	C_{LF} ($F\,cm^{-2}$)	f_{LF} (Hz)	R_p ($\Omega\,cm^2$)	R_{Total} ($\Omega\,cm^2$)
750	0.423	0.449	4.1×10^{-3}	87	0.295	1.093	0.493	0.743	1.167
800	0.348	0.225	3.1×10^{-3}	231	0.368	0.838	0.516	0.593	0.941
865	0.226	0.211	5.0×10^{-3}	151	0.377	0.717	0.587	0.589	0.814
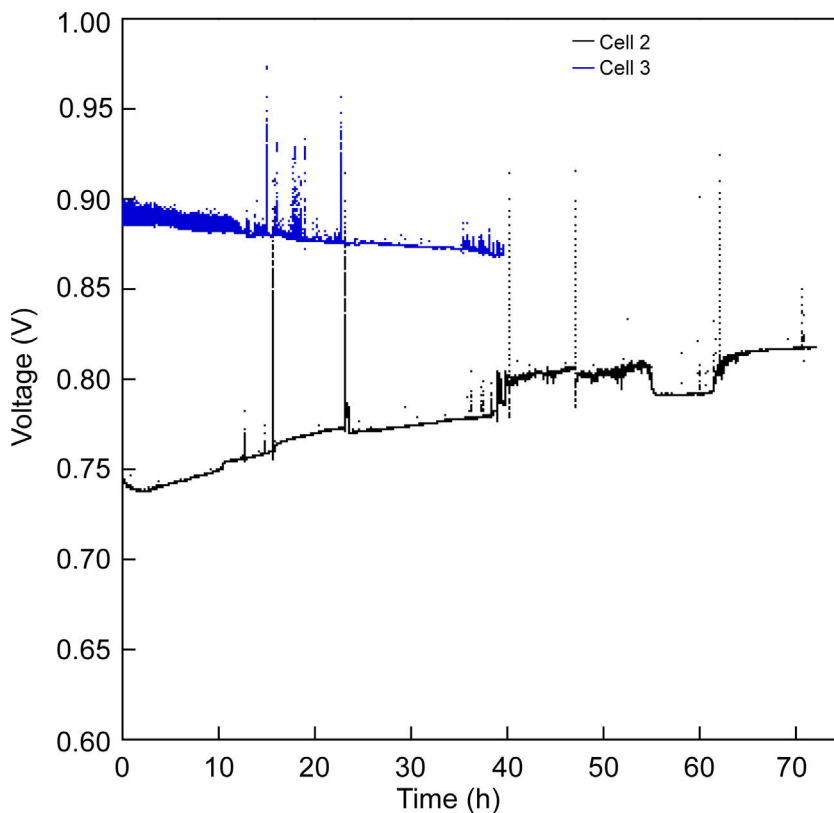
Fig. 7 – Constant current study of the cell 2 and cell 3 at 100 mA/cm² and 800 °C (cell voltage vs operating time).

generally associated with gas phase diffusion processes, has been masked by the low frequency charge transfer contribution (480 Hz) usually associated with the oxygen reduction reaction, ORR (10^2–10^3 Hz) [33]. In the case of the cell 2, the obtained resistances for both, the high and low frequency arcs, have been significantly lower than those obtained in cell 1. In this case, the inverse relaxation times, 683 and 2.34 Hz, could be related with the ORR and gas phase diffusion processes, respectively. In addition, it can be concluded that the major contribution to the polarization resistance is due to the gas phase diffusion process associated with the low frequency arc (2.34 Hz) [33]. Regarding the cell 3, the resistances at high and low frequencies are reduced due to the incorporation of LSF/LNF and LNF layers, which are partially replacing the LSF thickness (from 75 μm to 20 μm). In addition, the obtained maximum frequencies are similar to the obtained in the case of cell 2. The reduction of the obtained resistances is probably due to the fact that the use of these two layers improves
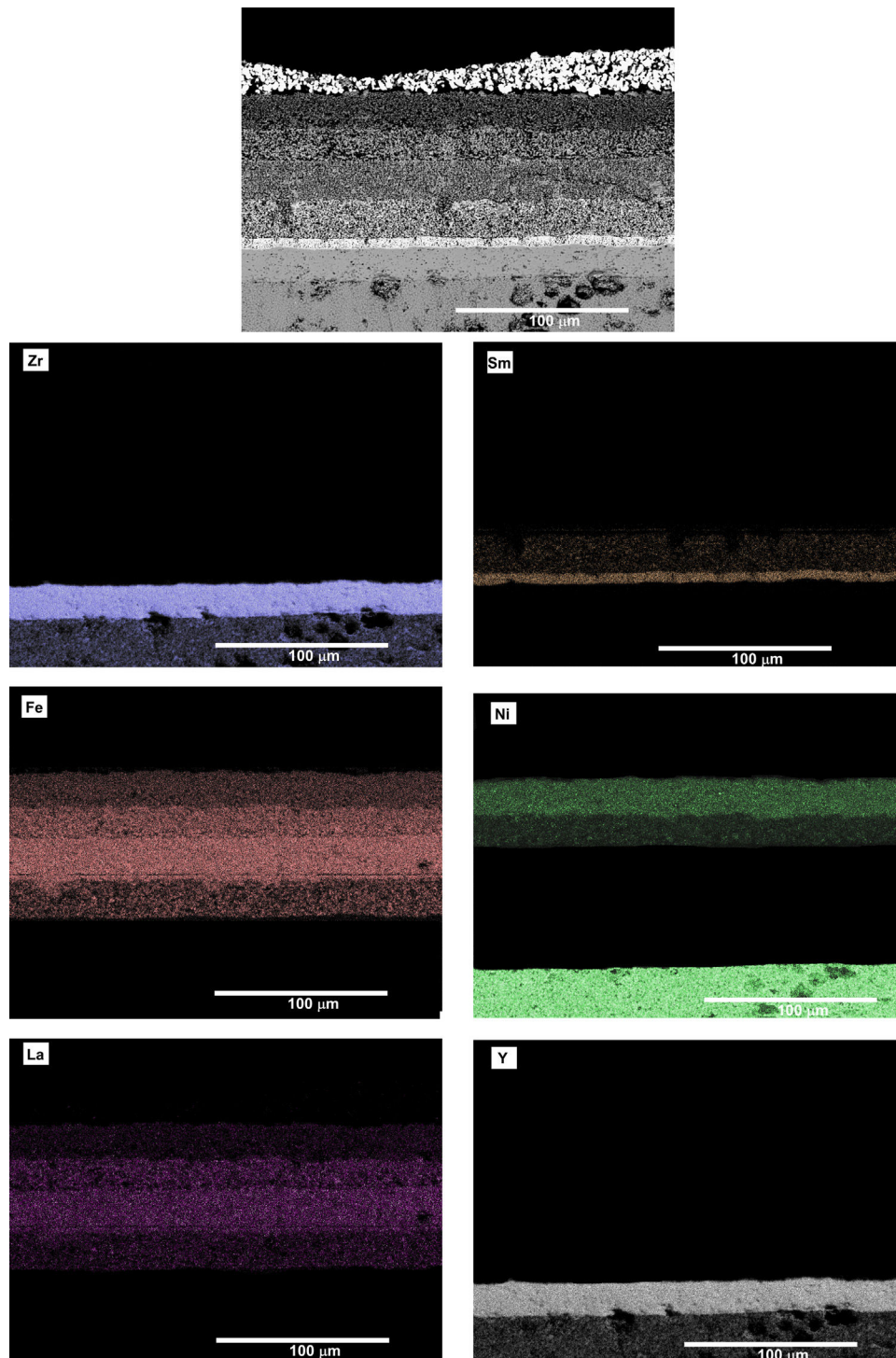
Fig. 8 – Cross section SEM image and EDX mapping of the sample cell 3.

the joint of the oxygen electrode with the Pt that acts as current collector. It is important to mark that the decrease of R_{LF} value between the cells 2 and 3 (1.10 and 0.368 Ω cm^2, respectively) could be consequence of the replacement of LSF by LSF/LNF and LNF with porosities of 23–25, 30 and 35%, respectively. These porosities were estimated from the differences between the measured thin film thicknesses (observed in the SEM micrographs) and the calculated thicknesses for the weight deposited by wet powder spraying. The increase of the overall porosity and the reduction of the total thickness of the cathode side could be responsible for the observed improvement in the gas phase diffusion process associated to R_{LF} reduction. In addition, the R_{LF} values could be influenced by small differences in the platinum paste thicknesses from one cell to other which have been deposited through brush method.

The characteristic current–voltage curves and the corresponding power densities of the cell 3 are expressed in Fig. 6a, measured at 750, 800 and 865 °C. As can be seen, the cell with LSF/LNF composite and LNF layers delivered power densities of 175, 222 and 272 mW cm^{-2} at 750, 800 and 865 °C, respectively, which are lower values than those can be found for anode supported cells in the bibliography [6,34]. Nyquist EIS plots of cell 3 are shown in Fig. 6b. In Table 4 can be seen that the R_p values, determined from the subtraction between the intersection values with the Z real axis (Z_{re}) at high and low frequencies of the impedance spectra, decrease when the operating temperature increases, from 0.743 Ω cm^2 measured at 750 °C to 0.589 Ω cm^2 measured at 865 °C. At this point it is important to note that when the operating temperature increases from 750 to 800 °C, a moderate improvement of the cell's electrochemical performance is observed mainly associated with the high frequency response (ORR reactions). However, when the operation temperature was increased from 800 to 865 °C the overall polarization resistance was keeping almost constant being the main improvement related with the ohmic contribution. Fact which is in good agreement to the results previously reported by Sun et al. where they showed that the optimal operating temperature for the LSF cathode is around 800 °C [28,35].

Stability study

In order to evaluate the stability of the cells, different short-term experiments were performed. The cell 2 was tested under a constant current of 100 mA/cm^2 for 72 h at 800 °C (Fig. 7). After 72 h, the voltage value increased from 0.74 to 0.81 V at 800 °C. This increase could be due to a reduction in the electrode activation, probably induced to a greater extent by the cathodic current passage along the oxygen electrode, which, as is known, produces enhancement in the cathodes performance [36,37]. The increase in voltage under constant current not only indicates a suitable degradation behaviour, but also that the microstructure of the anode and LSF cathode is adequate.

The same experimental procedure was used in cell 3 for the short-term stability study. As can be seen in Fig. 7, the degradation behaviour of cell 3 changed respect to cell 2, since the voltage decreased from 0.896 V to 0.870 V (3%) after 40 h of constant current–voltage at 800 °C. Since the cell configuration

is the same until the cathode layer, the observed difference respect to the cell 2 could be associated with the insertion of the LSF–LNF and LNF layers, which improved the first electrochemical response due to better contact with the platinum. However, they tend to degrade more rapidly than the LSF cathode.

Both cells were removed from the Probostat button-cell test rig after the short-term study. The cells were entire and with no evident damage. Therefore, serious damages were absent after 40 h of test. However, from the observation of the SEM micrographs (Fig. 8), a loss of contact between Pt paste and the contact layer (LNF) in the cell 3 is evident. On the other hand, the other layers remained continuous and retained their adhesion. The EDX maps show that regarding the compositional analysis, there was a uniform distribution in each layer, without a significant inter diffusion of elements between the different layers. The loss of contact between the platinum and LNF layers observed in the SEM micrograph of Fig. 8 could be due the origin of the degradation behaviour observed in Fig. 7.

Conclusions

Five compounds (Ni–YSZ, YSZ, SDC, LSF and LNF) commonly used in SOFC, have been synthesized through the reproducible and low-cost glycine nitrate synthesis method, obtaining nanometric particles in a controlled way.

The self-synthesized powders have been properly processed, using the simple and cost-effective techniques of pressing and wet powder spraying, and subsequently electrochemically characterized by the use of *I–V–P* curves and electrochemical impedance spectroscopy measurements. It should be noted that the anode and the electrolyte have been sintered together, achieving the required cell properties keeping it flat. Subsequently, the electrochemistry has been analyzed demonstrating that the use of LSF and LNF results in a higher power density and a reduction of the total cell resistance. Interestingly, the incorporation of LSF/LNF and LNF layers, has reduced the total resistance with respect to cell 2.

Moreover, a short-term degradation study under 100 mA/cm^2 constant current has been carried out. The results obtained for cell 2, composed by Ni–YSZ/YSZ/SDC/SDC–LSF/LSF, have demonstrated an adequate degradation behaviour after 72 h of operation at 800 °C. In the case of cell 3, composed by Ni–YSZ/YSZ/SDC/SDC–LSF/LSF/LSF–LNF/LNF, a voltage loss of 3% has been detected after 40 h at 800 °C. In addition, a post mortem analysis of cell 3 has shown that the main cause of the cell degradation could be a bad contact between the electrodes and the platinum, and not a structural or compositional change in the components.

Currently, our research group is working on facing this degradation problem by implementing an improved method to deposit the platinum paste which acts as current collector in the fabricated devices. In addition, small changes in the LNF and platinum paste sintering temperatures will be performed in order to find the best temperatures for the reduction of the degradation phenomena and to improve the contact between them.

Acknowledgements

R E F E R E N C E S

[1] J.C. Ruiz-Morales, D. Marrero-Lopez, J. Canales-Vazquez, J.T.S. Irvine, Symmetric and reversible solid oxide fuel cells, RSC Adv. 1 (2011) 1403–1414, http://dx.doi.org/10.1039/c1ra00284h.

[2] P.E. Dodds, I. Staffell, A.D. Hawkes, F. Li, P. Grünewald, W. McDowall, P. Ekins, Hydrogen and fuel cell technologies for heating: a review, Int. J. Hydrogen Energy 40 (2015) 2065–2083, http://dx.doi.org/10.1016/j.ijhydene.2014.11.059.

[3] V. Gil, J. Gurauskis, R. Campana, R.I. Merino, A. Larrea, V.M. Orera, Anode-supported microtubular cells fabricated with gadolinia-doped ceria nanopowders, J. Power Sources 196 (2011) 1184–1190, http://dx.doi.org/10.1016/j.jpowsour.2010.08.093.

[4] L.S. Mahmud, A. Muchtar, M.R. Somalu, Challenges in fabricating planar solid oxide fuel cells: a review, Renew. Sust. Energ. Rev. 72 (2017) 105–116, http://dx.doi.org/10.1016/j.rser.2017.01.019.

[5] D. Yan, L. Liang, J. Yang, T. Zhang, J. Pu, B. Chi, J. Li, Performance degradation and analysis of 10-cell anode-supported SOFC stack with external manifold structure, Energy 125 (2017) 663–670, http://dx.doi.org/10.1016/j.energy.2016.12.107.

[6] X. Nguyen, C. Chang, G. Jung, S. Chan, C. Yeh, J. Yu, C. Lee, Improvement on the design and fabrication of planar SOFCs with anode-supported cells based on modified button cells, Renew. Energy 129 (2018) 806–813, http://dx.doi.org/10.1016/j.renene.2017.03.070.

[7] J. Kupecki, R. Kluczowski, D. Papurello, A. Lanzini, M. Kawalec, M. Krauz, M. Santarelli, Characterization of a circular 80 mm anode supported solid oxide fuel cell (AS-SOFC) with anode support produced using high-pressure injection molding (HPIM), Int. J. Hydrogen Energy (2018), http://dx.doi.org/10.1016/j.ijhydene.2018.02.143.

[8] A. Tarancon, Strategies for lowering solid oxide fuel cells operating temperature, Energies 2 (2009) 1130–1150, http://dx.doi.org/10.3390/en20401130.

[9] C. Herring, Effect of change of scale on sintering phenomena, J. Appl. Phys. 21 (1950) 301–303, http://dx.doi.org/10.1063/1.1699658.

[10] N.K. Patel, S.R. Bishop, R.G. Utter, D. Das, M. Pecht, Failure modes, mechanisms, effects, and criticality analysis of ceramic anodes of solid oxide fuel cells, Electronics 7 (2018) 323, http://dx.doi.org/10.3390/electronics7110323.

[11] F. Ramadhani, M.A. Hussain, H. Mokhlis, S. Hajimolana, Optimization strategies for solid oxide fuel cell (SOFC) application: a literature survey, Renew. Sust. Energ. Rev. 76 (2017) 460–484, http://dx.doi.org/10.1016/j.rser.2017.03.052.

[12] I. Kosacki, C.M. Rouleau, P.F. Becher, J. Bentley, D.H. Lowndes, Nanoscale effects on the ionic conductivity in highly textured YSZ thin films, Solid State Ion. 176 (2005) 1319–1326, http://dx.doi.org/10.1016/j.ssi.2005.02.021.

[13] S. Kim, H. Moon, S. Hyun, J. Moon, J. Kim, H. Lee, Nano-composite materials for high-performance and durability of solid oxide fuel cells, J. Power Sources 163 (2006) 392–397, http://dx.doi.org/10.1016/j.jpowsour.2006.09.015.

[14] H.L. Tuller, Ionic conduction in nanocrystalline materials, Solid State Ion. 131 (2000) 143–157, http://dx.doi.org/10.1016/S0167-2738(00)00629-9.

[15] D.A. Corona-Martínez, J.C. Rendón-Angeles, L.A. Gonzalez, Z. Matamoros-Veloza, K. Yanagisawa, A. Tamayo, J.R. Alonso, Controllable synthesis of $BaCuSi_2O_6$ fine particles via a one-pot hydrothermal reaction with enhanced violet colour hue, Adv. Powder Technol. 30 (2019) 1473–1483, http://dx.doi.org/10.1016/j.apt.2019.04.023.

[16] P. Duran, C. Moure, J.R. Jurado, Sintering and microstructural development of Ceria–Gadolinia dispersed powders, J. Mater. Sci. 29 (1994) 1940–1948, http://dx.doi.org/10.1007/BF00351318.

[17] S. Hajarpour, K. Gheisari, A. Honarbakhsh Raouf, Characterization of nanocrystalline $Mg_{0.6}Zn_{0.4}Fe_2O_4$ soft ferrites synthesized by glycine–nitrate combustion process, J. Magn. Magn. Mater. 329 (2013) 165–169, http://dx.doi.org/10.1016/j.jmmm.2012.10.023.

[18] X. Wang, M. Qin, F. Fang, B. Jia, H. Wu, X. Qu, A.A. Volinsky, Effect of glycine on one-step solution combustion synthesis of magnetite nanoparticles, J. Alloy Compd. 719 (2017) 288–295, http://dx.doi.org/10.1016/j.jallcom.2017.05.187.

[19] A. Sutka, G. Mezinskis, Sol–gel auto-combustion synthesis of spinel-type ferrite nanomaterials, Front. Mater. Sci. 6 (2012) 128–141, http://dx.doi.org/10.1007/s11706-012-0167-3.

[20] M.P. Carpanese, A. Barbucci, G. Canu, M. Viviani, $BaCe_{0.85}Y_{0.15}O_{2.925}$ dense layer by wet powder spraying as electrolyte for SOFC/SOEC applications, Solid State Ion. 269 (2015) 80–85, http://dx.doi.org/10.1016/j.ssi.2014.11.014.

[21] M. Morales, M.E. Navarro, X.G. Capdevila, J.J. Roa, M. Segarra, Processing of graded anode-supported micro-tubular SOFCs based on samaria-doped ceria via gel-casting and spray-coating, Ceram. Int. 38 (2012) 3713–3722, http://dx.doi.org/10.1016/j.ceramint.2012.01.015.

[22] A. Wain-Martin, A. Morán-Ruiz, M.A. Laguna-Bercero, R. Campana, A. Larrañaga, P.R. Slater, M.I. Arriortua, SOFC cathodic layers using wet powder spraying technique with self synthesized nanopowders, Int. J. Hydrogen Energy 44 (2019) 7555–7563, http://dx.doi.org/10.1016/j.ijhydene.2019.01.220.

[23] M.J. López-Robledo, M.A. Laguna-Bercero, A. Larrea, V.M. Orera, Reversible operation of microtubular solid oxide cells using $La_{0.6}Sr_{0.4}Co_{0.2}Fe_{0.8}O_{3-\delta}$–$Ce_{0.9}Gd_{0.1}O_{2-\delta}$ oxygen electrodes, J. Power Sources 378 (2018) 184–189, http://dx.doi.org/10.1016/j.jpowsour.2017.12.035.

[24] K. Vidal, A. Larrañaga, A. Morán-Ruiz, A.T. Aguayo, M.A. Laguna-Bercero, M.P. Yeste, J.J. Calvino, M.I. Arriortua, Effect of synthesis conditions on electrical and catalytical properties of perovskites with high value of A-site cation size mismatch, Int. J. Hydrogen Energy 41 (2016) 19810–19818, http://dx.doi.org/10.1016/j.ijhydene.2016.02.088.

[25] A. Martínez-Amesti, A. Larrañaga, L.M. Rodríguez-Martínez, M.L. Nó, J.L. Pizarro, A. Laresgoiti, M.I. Arriortua, Chemical compatibility between YSZ and SDC sintered at different atmospheres for SOFC applications, J. Power Sources 192 (2009) 151–157, http://dx.doi.org/10.1016/j.jpowsour.2009.02.011.

[26] P. Coddet, J. Vulliet, C. Richard, A. Caillard, A. Thomann, Characteristics and properties of a magnetron sputtered gadolinia-doped ceria barrier layer for solid oxide electrochemical cells, Surf. Coat. Technol. 339 (2018) 57–64, http://dx.doi.org/10.1016/j.surfcoat.2018.01.079.

[27] J.H. Zhu, H. Ghezel-Ayagh, Cathode-side electrical contact and contact materials for solid oxide fuel cell stacking: a

review, Int. J. Hydrogen Energy 42 (2017) 24278–24300, http://dx.doi.org/10.1016/j.ijhydene.2017.08.005.

[28] A. Morán-Ruiz, K. Vidal, M.Á. Laguna-Bercero, A. Larrañaga, M.I. Arriortua, Effects of using $(La_{0.8}Sr_{0.2})_{0.95}Fe_{0.6}Mn_{0.3}Co_{0.1}O_3$ (LSFMC), $LaNi_{0.6}Fe_{0.4}O_{3-\delta}$ (LNF) and $LaNi_{0.6}Co_{0.4}O_{3-\delta}$ (LNC) as contact materials on solid oxide fuel cells, J. Power Sources 248 (2014) 1067–1076, http://dx.doi.org/10.1016/j.jpowsour.2013.10.031.

[29] A. Wain-Martin, A. Morán-Ruiz, K. Vidal, A. Larrañaga, M.A. Laguna-Bercero, M.I. Arriortua, Scalable synthetic method for SOFC compounds, Solid State Ion. 313 (2017) 52–57, http://dx.doi.org/10.1016/j.ssi.2017.08.021.

[30] M. Rieu, R. Sayers, M.A. Laguna-Bercero, S.J. Skinner, P. Lenormand, F. Ansart, Investigation of graded $La_2NiO_{4+\delta}$ cathodes to improve SOFC electrochemical performance, J. Electrochem. Soc. 157 (2010) B477–B480, http://dx.doi.org/10.1149/1.3298439.

[31] W. Bao, Q. Chang, G. Meng, Effect of NiO/YSZ compositions on the co-sintering process of anode-supported fuel cell, J. Membr. Sci. 259 (2005) 103–109, http://dx.doi.org/10.1016/j.memsci.2005.03.009.

[32] R. Campana, R.I. Merino, A. Larrea, I. Villarreal, V.M. Orera, Fabrication, electrochemical characterization and thermal cycling of anode supported microtubular solid oxide fuel cells, J. Power Sources 192 (2009) 120–125, http://dx.doi.org/10.1016/j.jpowsour.2008.12.107.

[33] J. Kim, G. Kim, J. Moon, Y. Park, W. Lee, K. Kobayashi, M. Nagai, C. Kim, Characterization of LSM–YSZ composite electrode by ac impedance spectroscopy, Solid State Ion. 143 (2001) 379–389, http://dx.doi.org/10.1016/S0167-2738(01)00877-3.

[34] W.H. Kim, H.S. Song, J. Moon, H.W. Lee, Intermediate temperature solid oxide fuel cell using $(La,Sr)(Co,Fe)O_3$-based cathodes, Solid State Ion. 177 (2006) 3011–3016, http://dx.doi.org/10.1016/j.ssi.2006.07.049.

[35] C. Sun, R. Hui, J. Roller, Cathode materials for solid oxide fuel cells: a review, J. Solid State Electrochem. 14 (2010) 1125–1144, http://dx.doi.org/10.1007/s10008-009-0932-0.

[36] M.A. Laguna-Bercero, A. Ferriz, A. Larrea, L. Correas, V.M. Orera, Long-term stability studies of anode-supported microtubular solid oxide fuel cells, Fuel Cells 13 (2013) 1116–1122, http://dx.doi.org/10.1002/fuce.201300063.

[37] S.P. Jiang, Y.D. Zhen, S. Zhang, Interaction between Fe–Cr metallic interconnect and $(La, Sr) MnO_3$/YSZ composite cathode of solid oxide fuel cells, J. Electrochem. Soc. 153 (2006) A1511–A1517, http://dx.doi.org/10.1149/1.2207060.